Journal of Structural Geology 67 (2014) 154–166

Contents lists available at ScienceDirect

Journal of Structural Geology

journal homepage: www.elsevier.com/locate/jsg

Fault structure and slip localization in carbonate-bearing normal faults: An example from the Northern Apennines of Italy

C. Collettini [a, b, *], B.M. Carpenter [b], C. Viti [c], F. Cruciani [d], S. Mollo [b], T. Tesei [b, d], F. Trippetta [a], L. Valoroso [b], L. Chiaraluce [b]

[a] Dipartimento di Scienze della, Terra Università La Sapienza di Roma, Roma, Italy
[b] Istituto Nazionale di Geofisica e Vulcanologia Roma, Italy
[c] Dipartimento di Scienze della Terra Università degli Studi di Siena, Italy
[d] Dipartimento di Fisica e Geologia, Università degli Studi di Perugia, Italy

ARTICLE INFO

Article history:
Received 15 February 2014
Received in revised form
14 July 2014
Accepted 18 July 2014
Available online 10 August 2014

Keywords:
Normal fault
Carbonates
Microstructures
Earthquakes

ABSTRACT

Carbonate-bearing normal faults are important structures for controlling fluid flow and seismogenesis within the brittle upper crust. Numerous studies have tried to characterize fault zone structure and earthquake slip processes along carbonate-bearing faults. However, due to the different scales of investigation, these studies are not often integrated to provide a comprehensive fault image. Here we present a multi-scale investigation of a normal fault exhumed from seismogenic depths. The fault extends for a length of 10 km with a maximum width of about 1.5 km and consists of 5 sub-parallel and interacting segments. The maximum displacement (370–650 m) of each fault segment is partitioned along sub-parallel slipping zones extending for a total width of about 50 m. Each slipping zone is characterized by slipping surfaces exhibiting different slip plane phenomena. Fault rock development is controlled by the protolith lithology. In massive limestone, moving away from the slip surface, we observe a thin layer (<2 cm) of ultracataclasite, cataclasite (2–10 cm) and fault breccia. In marly limestone, the fault rock consists of a cataclasite with hydrofractures and smectite-rich pressure solution seams. At the micro-nanoscale, the slip surface consists of a continuous and thin (<300 μm) layer composed of coarse calcite grains (~5–20 μm in size) associated with sub-micrometer grains showing fading grain boundaries, voids and/or vesicles, and suggesting thermal decomposition processes. Micrometer-sized calcite crystals show nanoscale polysynthetic twinning affected by the occurrence of subgrain boundaries and polygonalized nanostructures. Investigations at the kilometres-tens of meter scale provide fault images that can be directly compared with high-resolution seismological data and when combined can be used to develop a comprehensive characterization of seismically active fault structures in carbonate lithologies. Micro and nanoscale investigations along the principal slipping zone suggest that different deformation processes, including plastic deformation and thermal decomposition, were active during seismic slip.

1. Introduction

Carbonate-bearing faults are important structures for numerous reasons, including: a) half of the known petroleum reserves occur within carbonate reservoirs which likely contain faults (see Cooper, 2007; references therein; USGS, 2000), and b) significant earthquakes nucleate or propagate through thick sequences of carbonates that dominate the upper-crustal sedimentary sequences (e.g. Miller et al., 2004; Mirabella et al., 2008; Burchfiel et al., 2008; Chiaraluce, 2012; Govoni et al., 2014; Nissen et al., 2014). Our understanding of the mechanical and physical properties of fault zones depends on the knowledge of their internal structure (Sibson, 1977; Caine et al., 1996; Chester and Chester, 1998; Wibberley et al., 2008; Faulkner et al., 2010; Valoroso et al., 2014) and of the active deformation processes occurring at seismogenic depths (e.g., Sibson, 1977; Chester and Logan, 1986; Wintsch et al., 1995; Collettini and Holdsworth, 2004). However, quite often the scale of investigation plays a key-role in highlighting the numerous aspects of fault mechanics.

* Corresponding author. Dipartimento di Scienze della Terra Università La Sapienza di Roma, Piazzale Aldo Moro 5, 00185, Roma, Italy.
E-mail address: cristiano.collettini@uniroma1.it (C. Collettini).

http://dx.doi.org/10.1016/j.jsg.2014.07.017
0191-8141/

At the kilometre scale, field mapping and seismic reflection profiles provide fault images consisting of sub-parallel fault segments (Morley and Wonganan, 2000; Iacopini and Butler, 2011; Long and Imber, 2012) and/or multi-cored faults (Faulkner et al., 2003; Agosta and Aydin, 2006). Surface exposures of carbonate-bearing faults have been used to reconstruct a picture of a fault zone structure where much of the deformation is accommodated along a fault core, tens of centimetres to metres thick, surrounded by a damage zone of fractured host rock (Agosta and Kirschner, 2003; Billi et al., 2003; Micarelli et al., 2006; De Paola et al., 2008; Collettini et al., 2009). Microstructural data collected from exhumed carbonate-bearing structures suggest that the bulk of co-seismic displacement during earthquake slip is accommodated within highly localized slip zones less than a few millimetres thick (Smith et al., 2011; Collettini et al., 2013; Siman-Tov et al., 2013).

In this manuscript we present detailed observations of a carbonate-bearing fault from the kilometre scale down to the nanoscale in order to provide a comprehensive view of the fault zone structure and deformation processes.

2. Geological and tectonic setting

The Apennines are characterized by the presence of a complex pattern of thrusts, folds and normal faults, reflecting the superposition of two main tectonic phases: an upper Miocene–lower Pliocene compressional phase, forming E–NE verging thrusts and folds, and a super-imposed, upper Pliocene–Quaternary extensional phase, forming NNW–SSE trending normal faults (e.g. Elter et al., 1975; Barchi et al., 1998). These normal faults, that bound the intermountain basins of the area (Fig. 1), are the structures responsible of the largest historical (Intensity = XI, Basili et al., 2008) and instrumental earthquakes of the area (Boncio et al., 2000; Chiaraluce et al., 2003). Surface geology integrated with seismic reflection profiles indicate that the majority of the earthquakes of the area nucleate or propagate through thick sedimentary carbonatic sequences (e.g. Collettini et al., 2003; Miller et al., 2004; Chiaraluce et al., 2005; Ciaccio et al., 2005; Mirabella et al., 2008; Patacca et al., 2008).

The M. Maggio fault is a major structure located within the active alignment of the Apennines (Fig. 1) cutting across the carbonates of the Umbria-Marche sequence (e.g. Barchi et al., 1998). This sequence consists of sedimentary rocks deposited on a continental margin with basal late-Triassic evaporites (anhydrites and dolomites), lower-Jurassic platform carbonates (Calcare Massiccio formation) and Jurassic-Oligocene pelagic sequences. The M. Maggio fault is located in an area where regional uplift (e.g. D'Agostino et al., 2001; Serpelloni et al., 2013) and erosion overrides sedimentation. Along this structure, syntectonic sedimentary basins are absent and the fault shows in hangingwall and footwall blocks, the carbonates of the Umbria-Marche sequence. This type of

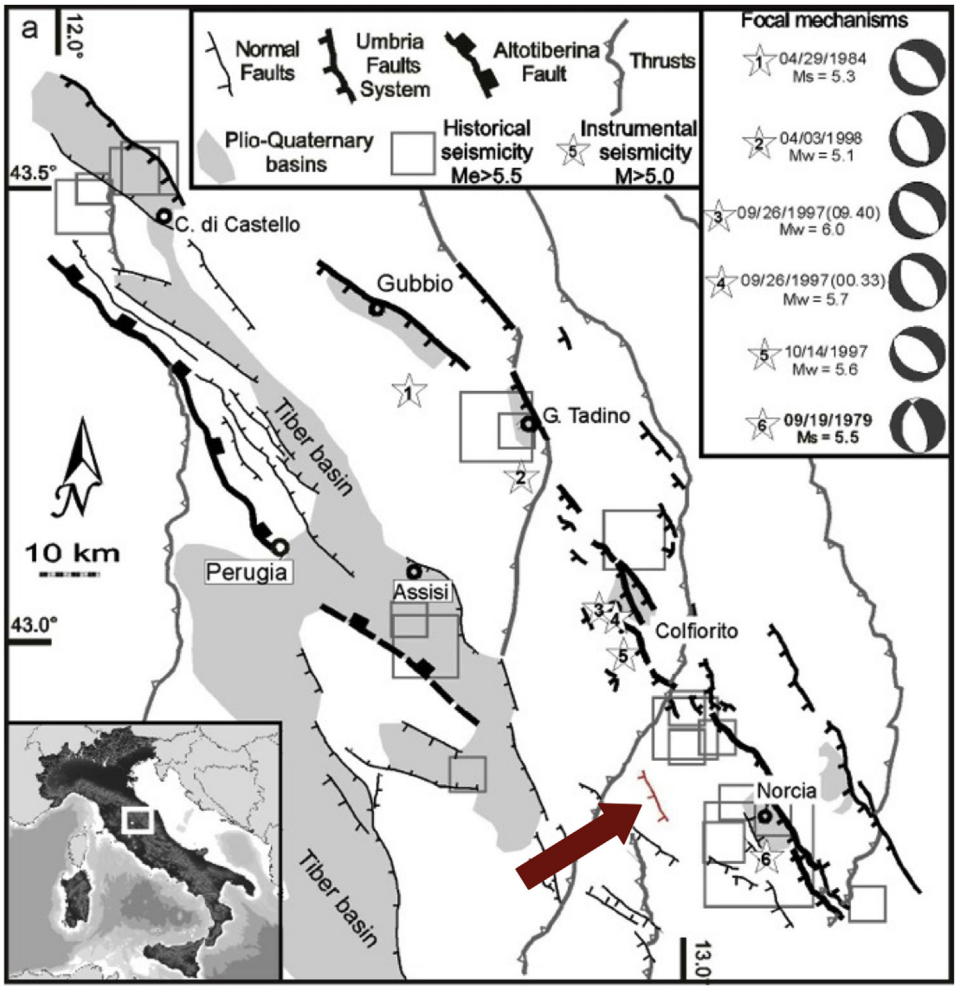

Fig. 1. Schematic structural map of the Umbria-Marche Apennines, showing the alignment of the intra-mountain basins along the Umbrian Fault System, UFS (after Collettini et al., 2003). The M. Maggio fault is indicated by the red arrow. (For interpretation of the references to colour in this figure legend, the reader is referred to the web version of this article).

fault exposure, juxtaposing two sedimentary substrates without Quaternary basin filling sediments in the hangingwall, represents an exhumed analogue of the fault rocks where, in the same area, seismic ruptures propagate and aftershocks nucleate (e.g. Chiaraluce et al., 2005; Mirabella et al., 2008). Therefore we use this field example to improve our understanding on fault zone structure and deformation mechanisms active at seismogenic depths.

3. Methods

At the kilometre scale, the M. Maggio fault has been investigated using detailed geological maps, 1:10.000 (Umbria region database). To characterize the along-strike evolution of fault displacement, we have constructed 9 geological cross sections perpendicular to the strike of the fault (Fig. 2). Slip plane phenomena (e.g. Stewart and Hancock, 1991) and fault rocks at the outcrop scale have been characterized in an exceptionally exposed outcrop where recent road work has exposed a new fault section (50 m long and more than 10 m high) unaffected by erosion and weathering processes. We then collected fault rock samples across the fault plane using a coring drill connected to a power supply. These cylindrical fault cores (10 cm in diameter) have been cut along planes parallel to the cylinder axes and high-resolution scans have been acquired. Thin sections of fault rocks, including the slip surface, have been obtained for Optical Microscope, OM, Scanning Electron Microscope, SEM (back-scattered electron BSE imaging), and Transmission Electron Microscope, TEM, analyses. For rock samples of the hangingwall block, where pressure solution seams are abundant,

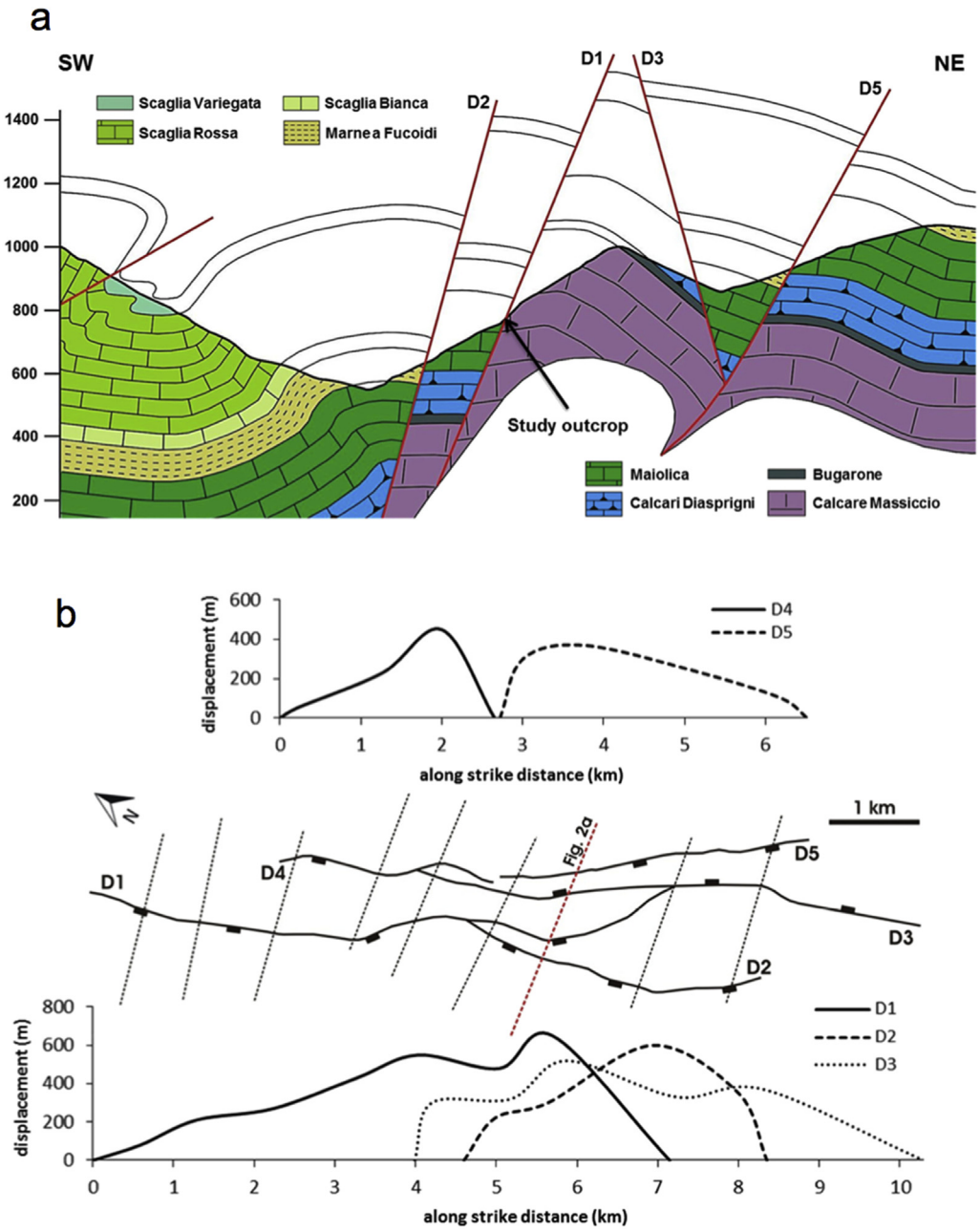

Fig. 2. (a) Geological cross section across the M. Maggio fault. (b) Displacement/length profiles of the different fault segments constructed using the geological maps (1:10.000) of the Umbria region database.

mineral phases have been determined using conventional X-Ray Powder Diffraction, XRPD, integrated with Thermo-Gravimetry, TG (Viti et al., 2014).

4. Fault structure

In describing the fault structure we have adopted the following terminology. At the kilometre scale, the parallel fault segments, both synthetic and antithetic, represent the *fault*. At the outcrop scale, the *slip surface* is the fault surface itself (Fig. 3a–g) where slip plane phenomena are documented and where much of the deformation is accommodated. The different fault rock material, up to 1 m thick, which sandwiches the slip surface, represents the *slip zone* (e.g. Smith et al., 2011). Slip surface phenomena are identified following and integrating the classification of Stewart and Hancock (1991), whereas fault rock materials are described following the classification scheme of Sibson (1977). The slip surface and slip zone form the *fault core*. At the micro-nanoscale, the slip surface consists of a thin (<300 μm) *Principal Slip Zone, PSZ* (Chester and Chester, 1998).

The fault is represented by several SW-dipping major fault segments and minor antithetic structures (Fig. 2). Along strike, fault length is ~10 km and the maximum width of the fault is ~1.5 km. A geological cross section constructed perpendicular to the study outcrop of the M. Maggio fault shows that the structure separates the Maiolica formation (lower Cretaceous) located in the hangingwall block from the Calcare Massiccio formation (lower Jurassic) in the footwall block (Fig. 2a). The Bugarone and Calcari Diasprigni formations (middle-upper Jurassic) are elided by the activity of the normal fault. The displacement of the fault, measured on the

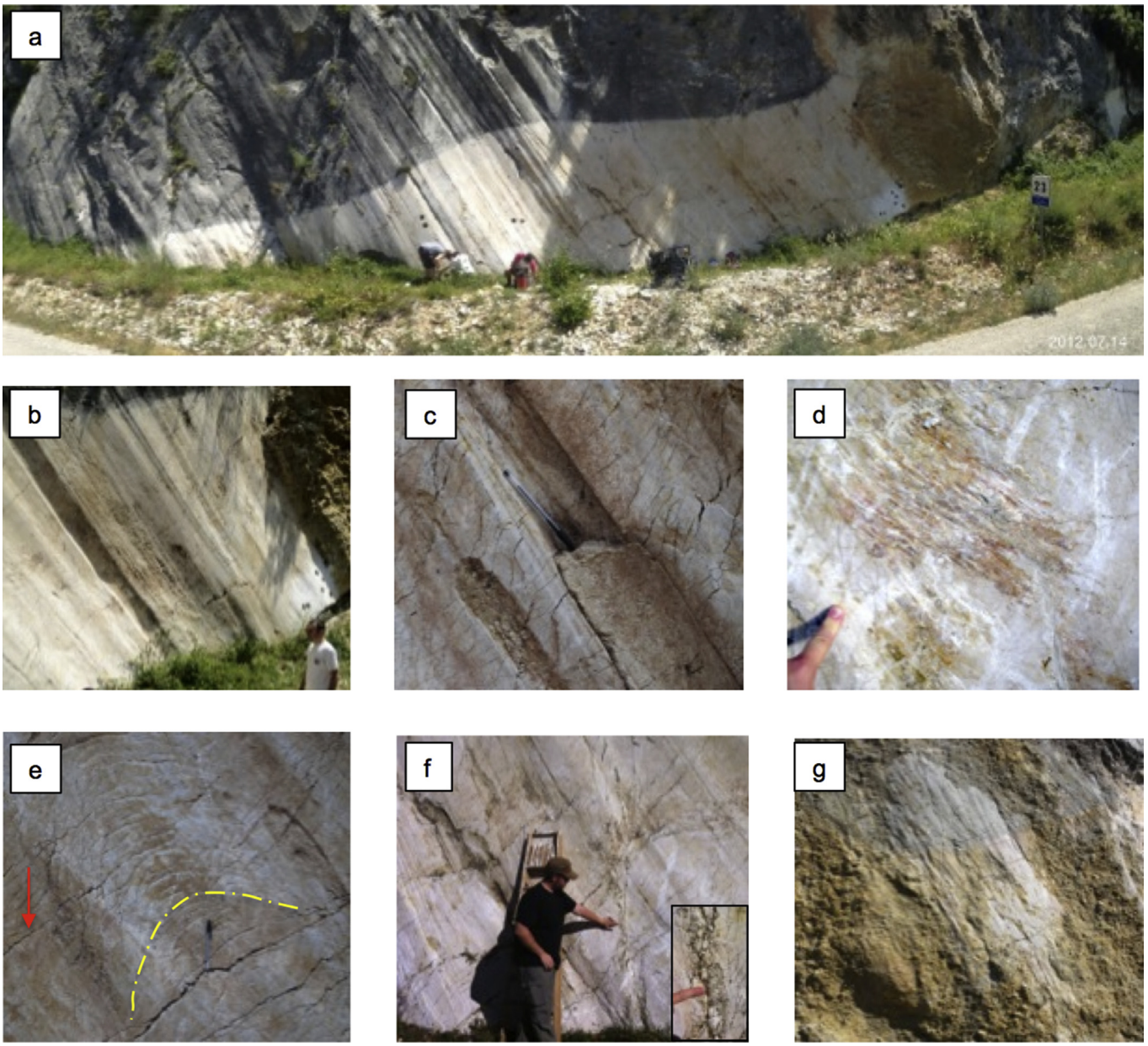

Fig. 3. Slip surface phenomena. (a) General view of one of the M. Maggio slip surface. (b) Grooves. (c) A groove filled with brecciated material. (d) Slikenlines. (e) Comb fractures (red arrow) and ring fractures (yellow dashed line). (f) A small displacement (few centimetres) vertical fault with associated fault breccia (inset). (g) Another slip surface parallel to the one presented in (a). (For interpretation of the references to colour in this figure legend, the reader is referred to the web version of this article).

geological cross section, is about 650 m (Fig. 2). Taking into account the thickness of the Umbria-Marche sedimentary sequence, fault exhumation can be evaluated to about 2 km. 8 additional geological cross sections parallel to the one described above have been used to evaluate the along-strike displacement profile of each fault segment (Fig. 2b). The maximum displacement of each segment ranges from 370 m (D5) to 650 m (D1). Most of the fault segments do not show the typical along strike displacement profile of isolated faults (e.g. Dawers et al., 1993) in which the displacement tapers off gradually towards the fault tip. Indeed, the displacements are distorted and denote a degree of interaction (e.g. Peacock and Sanderson, 1991; Scholz and Gupta, 2000; Cowie and Roberts, 2001), for example D4 and D5 show asymmetrical displacement profiles with higher fault tip taper angles where the two fault tips meet (Fig. 2b). In addition some fault segments are characterized by a high displacement/length ratios of about 0.16: D2 (600 m/3750 m) and D4 (450 m/2790 m). These values are a bit higher in comparison to the standard values, 0.1–0.001, obtained from a large number of faults with displacement ranging from some centimetres to several kilometres (e.g. Schlische et al., 1996; Scholz, 2002).

4.1. Slip surface phenomena

A typical aspect of the slip surface is decametre-long undulations of the slip plane, with the long axes oriented parallel to the slip direction. These features were defined as *corrugations* by Stewart and Hancock (1991) or *fault roughness* in recent fault mechanics terminology (e.g. Sagy et al., 2007). Details of the M. Maggio fault roughness, elaborated with ground-based LiDAR (Light Detection and Ranging), are presented in Brodsky et al. (2011). *Pluck-holes* are represented by decimetre-wide and deep cavities produced by side-wall plucking during fault movement (Fig. 3a and c bottom left). Predominant characteristics of the fault plane are grooves of different dimensions: small grooves are a few centimetre wide whereas some large grooves are 20 cm wide and more than 5 m long (Fig. 3b). Some grooves are filled with brecciated material derived from the hangingwall block (Fig. 3c). Frictional *wear striae* are present along the entire slip surface whereas *slikenlines* (Fig. 3d) made of calcite and iron oxides occur only along some portions of the fault plane. Some slikenlines show a change in direction during their growth (Fig. 3d). In some portions of the slip surface, in the proximity of some bulges of the fault topography, *circular fractures* occur (Fig. 3e). Some portions of the slip surface are characterized by *comb fractures* (Fig. 3e and f) that are open fractures, generally resulting from the intersection of the fault plane with the layer surfaces of the Calcare Massiccio formation located in the footwall block. Some of these comb fractures where reactivated as small shear zones, have displacement <2 cm and top-to-the-North shear sense. A few vertical faults, with associated fault breccia (Fig. 3f), disrupt locally the continuity of the fault plane. Due to the exceptional preservation of the M. Maggio fault plane and the limited amount of displacement, a few centimetres, associated to small shear fractures and vertical faults, we interpret these structures as later features resulting from small tectonic events occurring during the final stage of fault exhumation.

4.2. Fault rocks across the slip zone

Using about 15 cores that were collected perpendicular to the slip surface, we were able to investigate fault rock evolution in different portions of the slip zone and in both the hangingwall and footwall blocks.

In the hangingwall block, the fault rock is represented by a carbonate-rich cataclasite. Clay-rich pressure solution seams (stylolites) and calcite-rich veins with mutual crosscutting relationships are the other structural features of the fault rock (Fig. 4 with details in the orange box). Considering the shear couple acting

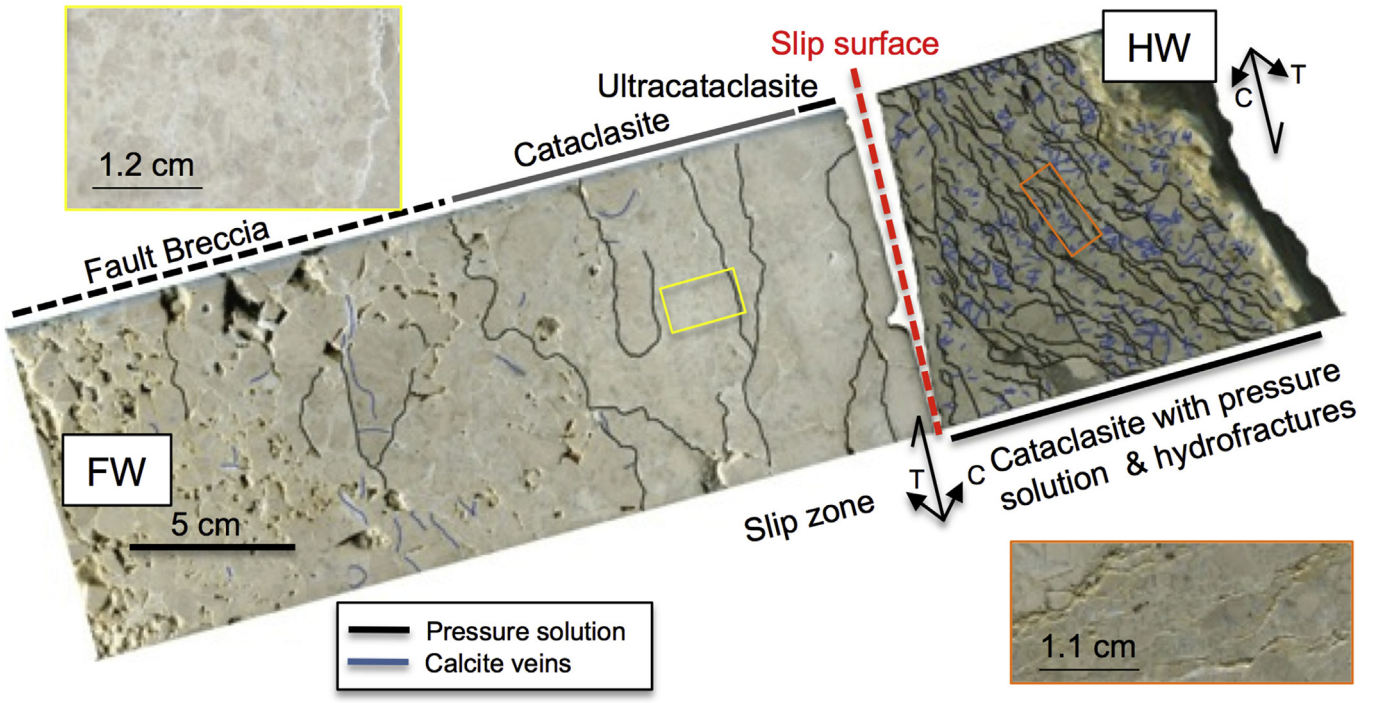

Fig. 4. Interpreted photo of slabbed core, drilled perpendicular through the fault zone. Hydrofractures and pressure solution seams developing in the marly limestones of the hangingwall block. Ultracataclasite, cataclasite and fault breccia in the massive limestones of the footwall block. Shear couple acting parallel to the slip of the shear zone (long black arrows), with compression, C, and tension, T, components.

parallel to the slip of the shear zone, pressure solution seams and calcite veins show a kinematic consistency with slip along the slip zone (e.g. Ramsay, 1967): pressure solution seams tend to form perpendicular to the compression component whereas veins are perpendicular the tension component (Fig. 4). These structural features indicate that during fault activity cataclasis, pressure solution and hydrofracturing with cementation were the main deformation processes in the slip zone of the hangingwall block.

In the footwall block, moving away from the slip surface, we have documented a thin zone, <2 cm, of ultracataclasite, a 2–10 cm thick cataclastic layer and fault breccia (Fig. 4). The ultracataclasite is a compact layer with a thickness in the range of 0.2–2 cm. Within this layer the larger clasts have dimensions of a few millimetres; in a few portions same clasts preserve the grainstone sedimentary texture typical of the Calcare Massiccio formation. In some locations, a pressure solution seam marks the limit between the ultracataclasites and cataclasite layer. The cataclasite layer has a thickness ranging from a few centimetres to nearly 10 cm. It consists of randomly oriented, sub-centimetric angular clasts with the grainstone sedimentary texture of the Calcare Massiccio formation, dispersed with a fine-grained calcite-rich ground mass (Fig. 4 with details in the yellow box). Fault breccia is represented by clasts of Calcare Massiccio separated by fractures, calcite rich veins and limited pressure solution seams. A characteristic of fault breccia is a higher degree of porosity in comparison to cataclasite and ultracataclasite layers. In some portions of the slip zone we have documented small displacement (<1 cm) fault planes both synthetic and antithetic to the major slip surface that merge into it.

4.3. Microstructures at OM

Microstructural analysis has focussed on the slip surface and on the adjacent fault rocks. In some exposures we have been able to collect hangingwall and footwall blocks together, including the slip surface (e.g. Fig. 5a). A very thin (<300 μm), sharp and continuous PSZ separates the hangingwall and footwall blocks (Fig. 5a and b).

The ultracataclasite of the footwall block consists of subrounded clasts of calcite with dimensions <500 μm and some calcite veins. Limited portions of the ultracataclasite layer show remnants of the original protolith that are consistent with the oolitic grainstone texture of the Calcare Massiccio (Scarsella, 1950; Santantonio, 1994). Other portions present calcite-rich veins or isolated calcite crystals, probably deriving from veins, that are affected by twining (Fig. 5d). Some fault parallel pressure solution seams are located near the PSZ.

The hangingwall block is characterized by a cataclasite with abundant pressure solution surfaces and calcite-rich veins. In some portions of the cataclasite, remnants of the protolith are present. The wackestone sedimentary texture including skeletal debris, echinoderms, small planctonic foraminifera, ostracods, coupled with the geology and stratigraphy of the area (cf. cross section in Fig. 2) allow identifying the basinal condensed sequence of the Bugarone formation, upper Jurassic-lower Cretaceous (Santantonio, 2006), as the protolith for the hangingwall fault rock. Pressure solution seams are brown-orange in colour and are rich in clay minerals (Viti et al., 2014). Some portions of the stylolites present clear evidences of dissolution processes since they dissolve part of the fossil material and veins (e.g. Fig. 5e). Calcite veins are organized in a fracture-mesh that is partially re-worked by both twinning and dissolution processes.

The PSZ (Fig. 5d and f) is represented by: 1) fault parallel calcite-rich veins that in some places are re-worked by twinning and cataclastic processes, 2) pressure solution seams that merge into the PSZ from the hangingwall block, and 3) calcite-rich ultracataclasite. An extremely sharp boundary separates the PSZ from the footwall ultracataclasite: this sharp plane abruptly truncates calcite clasts, some of them showing twinning surfaces (Fig. 5d). Parallel bands, made of ultracataclasite, calcite veins and brown-orange material characterize some portions of the PSZ (Fig. 5f).

4.4. Microstructures at SEM

Due to the chemical homogeneity of the footwall ultracataclasite, almost entirely formed by calcite grains, no microstructural details are detectable in the corresponding backscattered, BSE, images (Fig. 6a and b). In the hangingwall block, pressure solution seams (Fig. 6a and b) separate calcite-rich fault portions (calcite veins and carbonate clasts from the protolith). The pressure solution seams are mostly formed by Fe-rich smectitic clays, in nanosized and oriented (001) lamellae, enclosing relic calcite grains and insoluble minerals such as quartz, feldspars and detritic phyllosilicates (see details in Viti et al., 2014). The PSZ has a variable thickness, ranging from 50 to 300 μm (Fig. 6a): the boundary with the footwall block is sharp and more gradual with hangingwall block, due to the involvement of slip-parallel stylolitic surfaces into the PSZ (Fig. 6b). The PSZ consists of relatively coarse calcite grains (~5–20 μm in size) derived from the ultracataclasite, associated with sub-micrometer calcite grains that are concentrated along specific slipping planes or slip-elongated lenses. Some portions of the PSZ are completely replaced by sub-micrometer grains. Large ultracataclasite grains within the PSZ show lobate and fading grain boundaries, characterized by preferential concentration of voids and/or vesicles (black and dark grey rounded features in Fig. 6c). These features suggest probable thermal decomposition of calcite ($CaCO_3 \rightarrow CaO + CO_2$) occurring at temperature above 600 °C (e.g. Collettini et al., 2013). This process is mainly documented at grain and subgrain boundaries, but evidence for preferential calcite decomposition has also been observed along twinning planes of the ultracataclasite both within the PSZ and at the PSZ-footwall block contact (Fig. 6d).

4.5. Microstructures at TEM

TEM analyses have been carried out on Ar^+ ion-thinned grids of the PSZ layer. Coarse micrometer-sized calcite crystals commonly show nanoscale polysynthetic twinning (Fig. 7a and b), with twin lamellae up to 400 nm wide. Twin lamellae are characterized by complex TEM contrast suggesting intense strain, documented by high dislocation densities, and subgrain boundaries formation. Twinning planes are irregular and teeth-shaped (e.g., upper side of Fig. 7a), due to the pervasive occurrence of subgrain boundaries. This suggests that twinning predates *ductile* deformation, giving rise to dislocations, dislocations walls and subgrain boundaries. The PSZ locally consists of nanograins, typically up to 200–300 nm in size, with intense strain contrast features (Fig. 7c), probably representing the evolution of the nanostructures shown in Fig. 7a and b. These nanosized strained aggregates may also be enclosed within strain-free calcite veins (e.g., Fig. 7d). Lastly, TEM also revealed the occurrence of polygonalized nanostructures (Fig. 7e and details in De Paola et al., 2014), with close association of strain-free calcite crystals, up to 100 nm in size.

5. Discussion

In the following we highlight the main characteristics of M. Maggio fault from the kilometre down to the micro-nanoscale and focus the discussion on two main topics: a) the multiple slipping planes observed at different scales; and b) the possible timing of microstructure development.

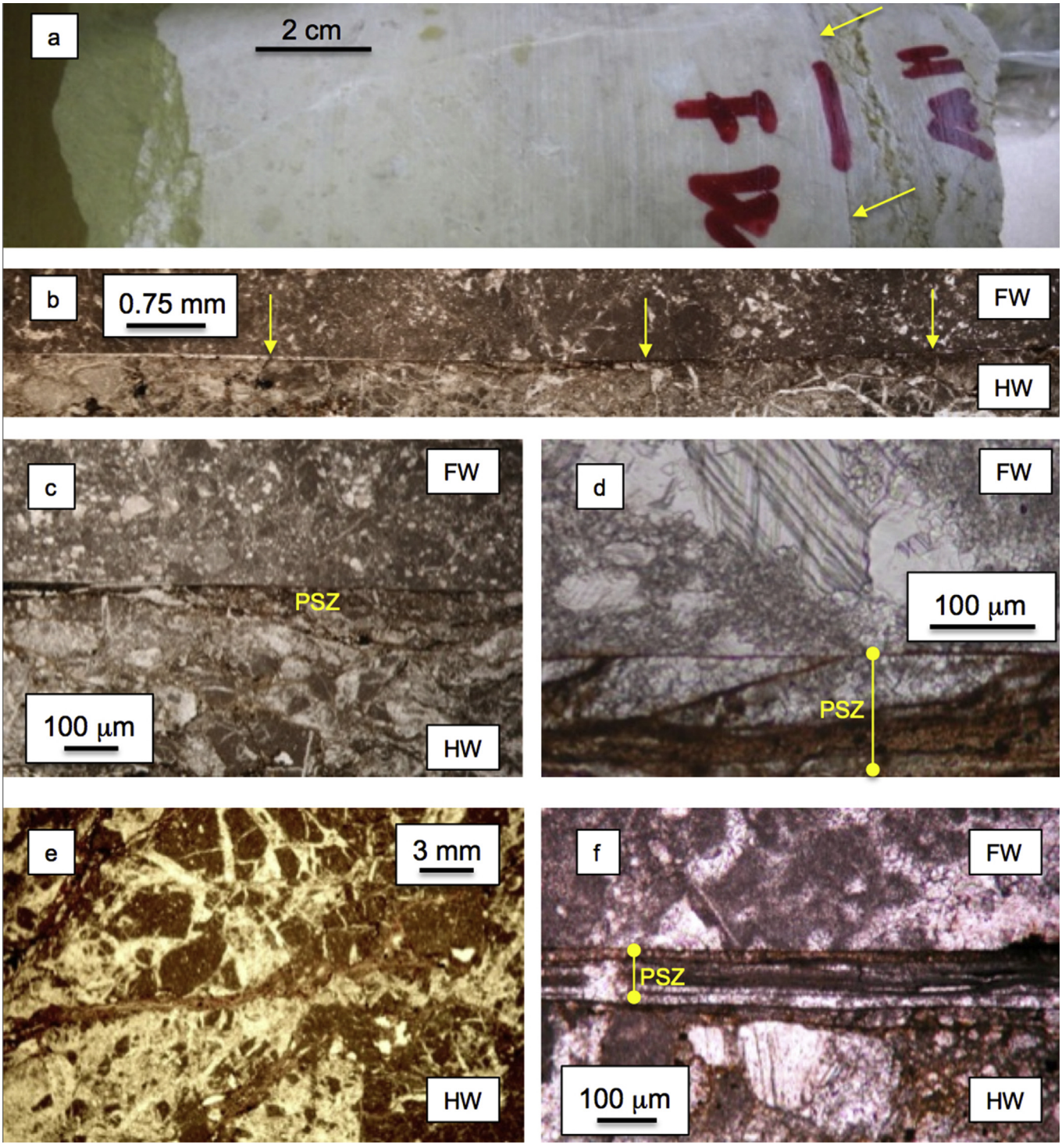

Fig. 5. (a) Rock sample including hangingwall, HW, and footwall, FW, blocks together with the principal slipping zone, PSZ, highlighted by the yellow arrows in Fig. a and b (b-c-d-f) Details of the principal slipping zone. (e) Hydrofracture system and pressure solution seams in the hangingwall cataclasite. (For interpretation of the references to colour in this figure legend, the reader is referred to the web version of this article).

5.1. Multiple slipping planes at different scales

In documenting the M. Maggio fault zone structure from the kilometre down to the microscale, the common theme linking these scales seems to be the multiple slipping planes.

At the kilometre scale, field studies (e.g. Tchalenko, 1970; Bonson et al., 2007) and high-resolution seismic reflection profiles (e.g. Morley and Wonganan, 2000) show that many normal faults are discontinuous structures, consisting of arrays of distinct segments. In general, fault growth occurs by segment linkage (e.g. Peacock and Sanderson, 1991; Cowie and Roberts, 2001) and the measured variability in the displacement/length ratio testifies to this fault growth process (Cowie and Scholz, 1992; Nicol et al., 1995; Maerten et al., 1999; Scholz and Gupta, 2000; Walsh et al., 2002;

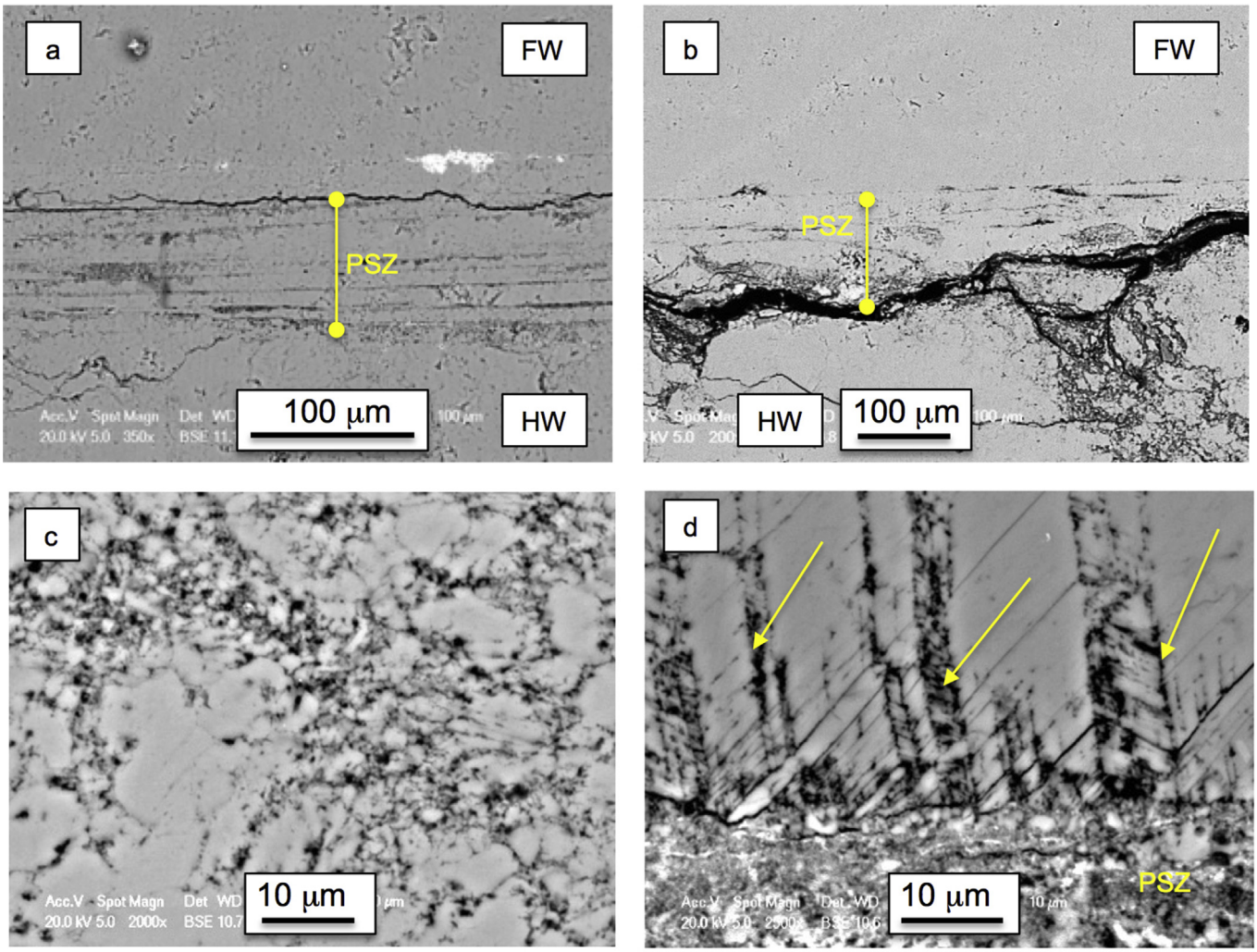

Fig. 6. Backscattered SEM images of the principal slipping zone, PSZ. (a), (b) Overview of the PSZ separating hangingwall (HW) and footwall (FW). (c) Details of calcite grains showing fading grain boundaries, with voids and vesicles, and disaggregation features. (d) Preferential occurrence of voids and vesicles along twinning and cleavage planes of calcite (indicated by yellow arrows). (For interpretation of the references to colour in this figure legend, the reader is referred to the web version of this article).

Cowie and Roberts, 2001). From geological mapping of the M. Maggio fault, we obtain a fault structure represented by 5 fault segments (D1–D5 in Fig. 2). Most of the segments do not show a displacement/length profile that tapers off gradually towards the fault tip. In addition, some fault segments are characterized by high displacement/length ratios. This may be related to the fact that the M. Maggio fault likely reactivated a pre-existing Jurassic normal fault, since in the area, the Jurassic condensed sequence made of Calcari Diasprigni and Bugarone crop out (Fig. 2a). Due to the involvement of Triassic evaporites, Jurassic normal faulting in the area was quite complex (e.g. De Paola et al., 2007). Therefore the multiple fault segments of the M. Maggio fault are likely the result of fault growth by segment linkage, reactivation of pre-existing Jurassic normal faults with important mechanical heterogeneities induced by the presence of evaporites.

A unique opportunity to observe a fault zone structure similar to M. Maggio, at the kilometre scale, is provided by the aftershock distribution of the L'Aquila 2009 M_W 6.1 normal faulting earthquake, which cuts across similar carbonate lithologies (Fig. 8 a and b, and Valoroso et al., 2014). ~19 k aftershocks, with relative earthquake location errors ranging from a few metres to tens of metres, define a fault zone structure with a thickness in the range of 0.5–1.5 km. Seismological data define sub-parallel fault segments with dip-slip kinematics and minor antithetic structures (Fig. 8b after Valoroso et al., 2014). As inferred from the displacement/length profiles of the M. Maggio fault, the activation of several parallel segments of the fault during the aftershock sequence suggests a degree of interaction (e.g. Nicol et al., 2010).

Outcrop studies, integrated with detailed geological cross sections, also define the presence of multiple slipping planes along the M. Maggio fault at the tens of meter scale (Fig. 8c). In geological cross section, the M. Maggio fault displaces the Maiolica formation (lower Cretaceous) located in the hangingwall block onto the Calcare Massiccio formation (lower Jurassic) in the footwall block (Fig. 2a). However, in the studied outcrop (Fig. 3) the fault zone is characterized by three sub-parallel major slipping zones and in the hangingwall block a cataclasite made of clasts belonging to the Bugarone formation is present (upper Jurassic-lower Cretaceous). This indicates that other sub-parallel slipping zones have to be present (Fig. 8c) in order to justify the Maiolica formation (lower Cretaceous) in the hangingwall block as reported in the geological map and cross section (Fig. 2). The cumulative displacement of 650 m for the M. Maggio fault is therefore partitioned along a fault zone consisting of major, parallel slipping zones distributed over a width of about 50 m (Fig. 8c). Similar broad zones of deformation (up to 100 m wide) made of complex arrays of anastomosing fault

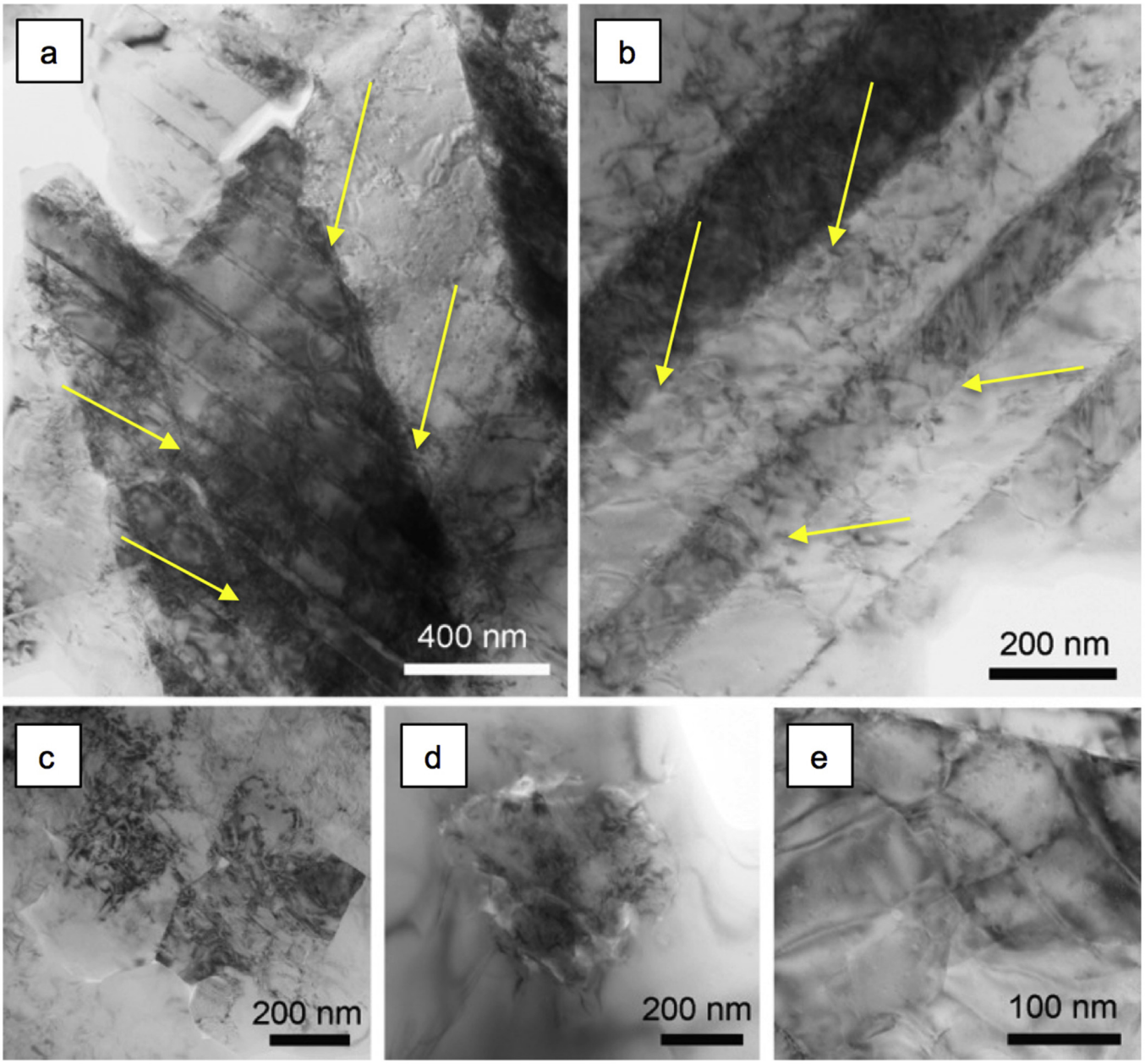

Fig. 7. TEM images from the PSZ: (a), (b) twin lamellae (yellow arrows) characterized by complex contrast and suggesting intense strain, documented by high dislocation densities, and subgrain boundaries formation. (c) A grain fragment with intense strain contrast features, surrounded by recrystallized calcite with lower dislocation density. (d) Nanosized strained aggregate enclosed within strain-free calcite veins. (e) Polygonalized nanostructures, with close association of strain-free calcite crystals. (For interpretation of the references to colour in this figure legend, the reader is referred to the web version of this article).

strands have been depicted for other normal faults in carbonates (e.g. Bonson et al., 2007) and reconstructed by seismic attribute analysis and mapping on 3D datasets of seismic reflection profiles (Iacopini and Butler, 2011). For the M. Maggio fault, each slipping plane is sandwiched within a slipping zone with different fault rock types (Fig. 8d). In massive limestones we observe a thin layer (about 2 cm thick) of indurated ultracataclasite that contains or bounds the PSZ (Fig. 4). Moving away from the ultracataclasite, we observe a 2–10 cm thick cataclastic layer that evolves into fault breccia. In marly limestone we have documented a cataclasite with significant clay rich pressure solution seams (details in Viti et al., 2014) and hydrofractures (e.g. Fig. 4). During the fault history, if we assume that the slip zone with the lowest strength is the one with the higher probability to slip, the contemporaneous activity of parallel slipping zones distributed over a width of about 50 m (e.g. Fig. 8c) would be the result of the evolution in strength with time. Numerous processes can influence strength evolution with time. Sealing processes due to fluid cementation significantly contribute to fault restrengthening during the inter-seismic period (e.g. Sibson, 1992). In addition, fault restrengthening in carbonate-bearing faults is also promoted by the high frictional healing of carbonates in comparison to other quartzo-feldspathic or phyllosilicate materials (Carpenter et al., 2013).

At the micron scale, we observe a 50–300 μm thick PSZ characterized by parallel slipping planes (Figs. 6a and 8e). Similar PSZ have been documented in high velocity friction experiments at co-

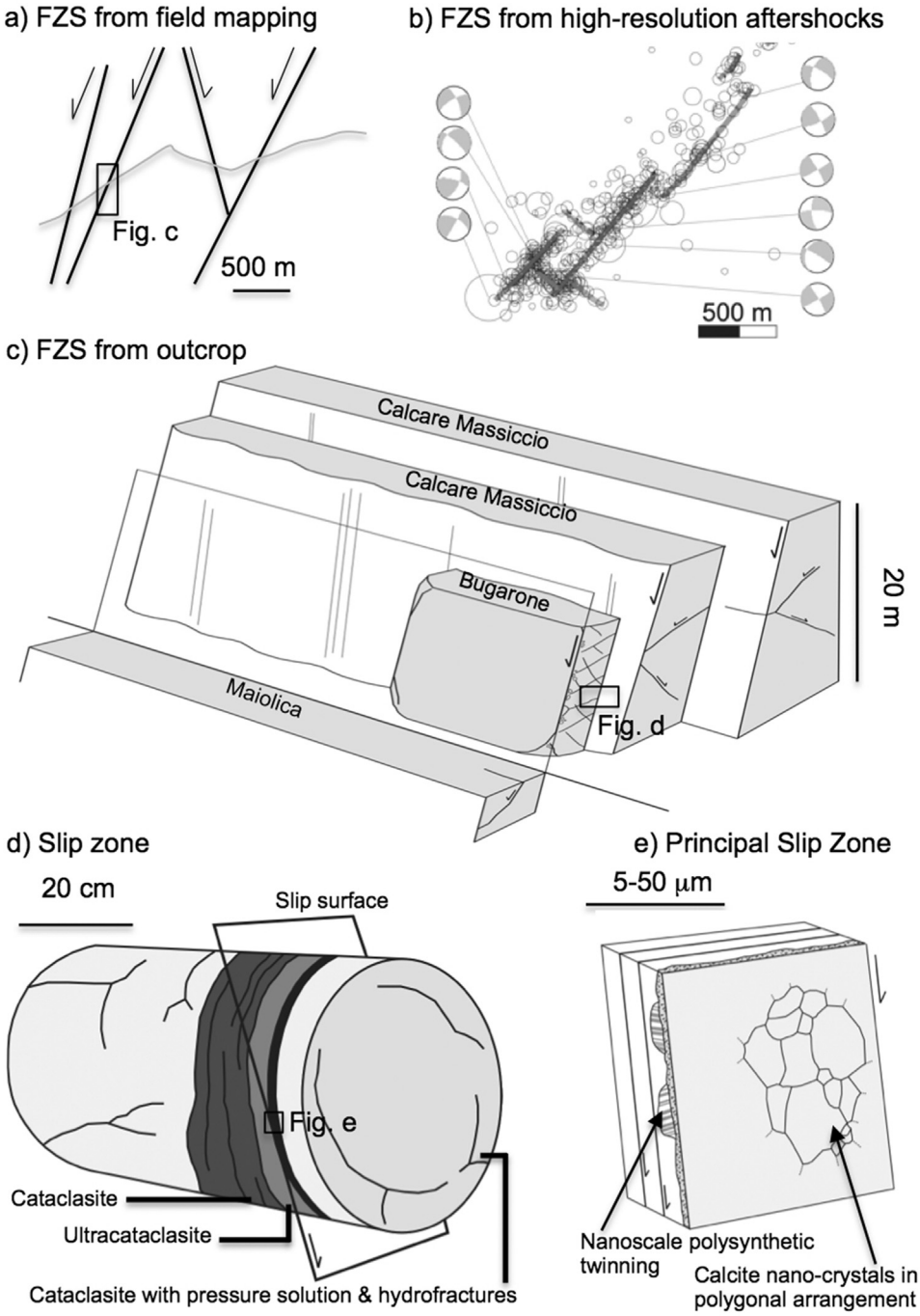

Fig. 8. (a–e) Fault zone structure, FZS, from the kilometre scale down to the nanoscale. (b) Fault zone structure and normal faulting kinematics as imaged by the L'Aquila 2009 aftershock distribution (Valoroso et al., 2014).

seismic slip velocities (Smith et al., 2013; De Paola et al., 2014). We suggest that the parallel PSZ (Fig. 8e), with evidences of thermal decomposition processes and plastic deformation, are formed during earthquake slip, however more studies are required to further constrain this working hypothesis.

To summarize, although the common theme linking observations from the kilometre down to the micron scale along the M. Maggio fault is the presence of multiple slipping planes, we suggest that different deformation mechanisms, including fault growth and interaction, strength evolution and co-seismic slip processes, are responsible for creating parallel slipping planes at different scales.

5.2. Possible timing of microstructures development

Our micro-nanoscale structural data on the fault rocks collected from the M. Maggio structure are the result of different deformation mechanisms active at different times during the seismic cycle and with different strain rates. Although it is not easy to discriminate between different deformation mechanisms, in particular along exhumed structures where fast and slow processes are superimposed in time, we attempt to divide microstructures into two groups. In one group we include the microstructures formed at the low strain rates typical of the interseismic, preseismic and

postseismic phases. Since these microstructures and processes have been extensively documented in the literature (e.g. Logan et al., 1979; Beeler et al., 1996; Gratier et al., 2013 for an extensive review on pressure solution creep), we only report on the microstructures documented along the M. Maggio fault. In the other group, we include the possible microstructures that may be associated with the coseismic slip phase and additionally provide a brief review for the recent literature on this topic.

Distributed deformation in cataclasites, such as those documented away from the PSZ (Figs. 4 and 5e), are likely related to low strain-rate processes as the velocity-weakening behaviour required to generate earthquake slip occurs only for slip localization (e.g. Logan et al., 1979; Beeler et al., 1996; Scuderi et al., 2013). Away from the PSZ, we observe microstructures diagnostic of dissolution and precipitation processes such as the smectite-rich pressure solution seams in the cataclasite from the marly protolith (Fig. 5e) or a few pressure solution surfaces in the cataclasite-ultracataclasite of the massive limestone (Fig. 4). Precipitation processes are well documented by the intense hydrofracture system and cementation affecting the marly cataclasite (Figs. 4 and 5e). The presence of an intense hydrofractures system, solely within the marly cataclasite (Fig. 4) points to: a) the important role played by clay-rich material in facilitating dissolution and precipitation processes within carbonates (e.g. Gratier et al., 2013; Viti et al., 2014) and b) the low permeability structure, represented by the cemented and extremely fine-grained ultracataclasite developed within the massive limestone (Fig. 4), thus providing a barrier for across-fault fluid flow.

In some portions of the PSZ we documented some PSZ-parallel hydrofractures. As we have documented microstructures likely related to thermal decomposition of carbonates during earthquake slip in the PSZ (e.g. Fig. 6c and d; and see also Collettini et al., 2013), there is the possibility that these hydrofractures result from thermal pressurization processes facilitated by decomposition of carbonates during earthquake slip. However, at the moment we do not have any constraints to discriminate if these hydrofractures within the PSZ formed during earthquake slip or in other phases of the seismic cycle.

In the last ten years, the microstructures observed in experimental faults formed during high-velocity friction experiments on carbonates (Han et al., 2007, 2010; De Paola et al., 2011; Smith et al., 2013; Violay et al., 2013; De Paola et al., 2014) have significantly contributed to: a) characterizing fault rock production during fast slip (e.g. slip velocity >50 cm/s) and b) inferring deformation mechanisms that are active during seismic slip. During earthquake slip, a number of thermally activated physicochemical processes are triggered by temperature rise during fast fault motion (e.g. Di Toro et al., 2011). In carbonate rocks these processes, which can be active simultaneously, include: flash heating, thermal decomposition and/or pressurization, nano-powder lubrication, and plastic deformation (Han et al., 2007; De Paola et al., 2011; Smith et al., 2013; Violay et al., 2013; Fondriest et al., 2013; but see also Verberne et al., 2013 for crystal plasticity in velocity weakening material at low sliding velocity). Driven by these new findings, different types of microstructures and inferred deformation mechanisms have been documented along ancient and exhumed carbonate bearing faults. Low aspect ratio carbonate grains combined with evidence of injection veins of carbonate cataclasite into the wall-rock have been related to thermal decomposition and fluidization of the fault zone (Rowe et al., 2012). Along a thin (≈500 μm) principal slipping zone of a regional thrust fault, thermal decomposition of calcite has been inferred by the occurrence of relict calcite grains, containing holes and vesicles, and newly formed calcite skeletal crystals (Collettini et al., 2013). Similar features have been documented along carbonate-bearing normal faults of the Apennines (Bullock et al., 2014). In other carbonate-bearing faults, a thin outer layer (≈1 μm) of nanoparticles formed from twinned calcite in micron-sized crystals has been documented (Siman-Tov et al., 2013). It has been proposed that this outer layer of nanograins explains the glossy and mirror appearance of the fault surface in the sense that the nanograins would cover the rougher surface of large crystals and smooth the fault surface itself (Siman-Tov et al., 2013). The micro and nanostructures observed along the M. Maggio fault seem to encompass several microstructures observed in high-velocity friction experiments and on carbonate-bearing exhumed faults (Fig. 8e). Along a thin (<300 μm) principal slipping zone, we observe disaggregation features that point to thermal decomposition processes. In addition nanograins are abundant and seem to be connected with or derive from twinned, micrometric crystals of calcite (e.g. Siman-Tov et al., 2013). Polygonal crystals of calcite (e.g. Fig 8e) appear to be present in some portions of the slipping zone (e.g. De Paola et al., 2011; Smith et al., 2013; De Paola et al., 2014). All these observations suggest that during past seismic slip along the M. Maggio fault, different deformation processes were active along the ultrathin, slipping zone, possibly simultaneously.

Finally, our multiscale study of the M. Maggio fault highlights the different images of a fault zone structure that an investigator can collect as a function of method of investigation and scale of observation. Each single fault image preserves vital information, and a comprehensive understanding of the mechanics of faulting relies on our ability to integrate different datasets and to find the right balance between processes observed at different length and time scales. Finally, since it is becoming widely accepted that earthquake slip processes occur on narrow (<1 mm) principal slipping zones, a detailed nano-structural investigation seems to be essential to improve our understanding of co-seismic slip processes.

6. Conclusions

We have studied, from the kilometre scale down to the nanoscale, a carbonate bearing normal fault cropping out along the active system of the Northern Apennines. The fault consists of 5, sub-parallel and partially overlapping fault segments extending for a length of 10 km and with a maximum width of about 1.5 km. The displacement/length profiles highlight a degree of interaction between the different segments. A similar fault zone structure is imaged by high-resolution aftershock locations of the L'Aquila 2009 M_W 6.1 normal faulting earthquake that occurred within similar carbonate lithologies (Valoroso et al., 2014). The cumulative displacement (370–650 m) of each fault segment is partitioned along sub-parallel slipping zones extending for a width of about 50 m. Each slipping zone is characterized by a prominent slipping surface that is affected by different slip plane phenomena, including pluck-holes, grooves, wear striae, circular cracks and comb fractures. Fault rock development is controlled by the protolith lithology (e.g. Tesei et al., 2013). In massive limestone, moving away from the slip surface, we observe a thin layer (<2 cm) of ultracataclasite, cataclasite (2–10 cm) and fault breccia. In marly limestone the fault rock consists of a cataclasite with hydrofractures and smectite-rich pressure solution seams. The principal slipping zone consists of continuous and thin (<300 μm) layer composed of coarse calcite grains (~5–20 μm in size) associated with sub-micrometer grains that are concentrated along specific slipping planes. We suggest that during seismic slip, different deformation processes were active along the slipping zone, possibly simultaneously: a) thermal decomposition is inferred by calcite grains showing lobate and fading grain boundaries, characterized by preferential concentration of voids and/or vesicles; b)

plastic deformation is documented by micrometer-sized calcite crystals showing nanoscale polysynthetic twinning affected by the occurrence of subgrain boundaries and polygonalized nanostructures, with close association of strain-free calcite crystals, up to 100 nm in size.

The common theme linking multiscale observations along the M. Maggio fault is the presence of multiple slipping planes, that are the result of different deformation mechanisms, including fault growth and interaction, strength evolution and co-seismic slip processes.

Acknowledgements

This research has been carried out within the ERC Starting Grant GLASS no. (259256). We thank M. Brandano and M. Santantonio for the help in the lithological characterization of the Bugarone and Calcare Massiccio formation. We thank R. Han, C. Wibberley and the Editor T. Takeshita for very constructive reviews.

References

Agosta, F., Aydin, A., 2006. Architecture and deformation mechanism of a basin-bounding normal fault in Mesozoic platform carbonates, central Italy. J. Struct. Geol. 28, 1445–1467. http://dx.doi.org/10.1016/j.jsg.2006.04.006.

Agosta, K., Kirschner, D.L., 2003. Fluid conduits in carbonate-hosted seismogenic normal faults in central Italy. J. Geophys. Res. 108, 2221–2234. http://dx.doi.org/10.1029/2002JB002013.

Barchi, M.R., Minelli, G., Pialli, G., 1998. The crop 03 profile: a synthesis of results on deep structures of the Northern Apennines. Mem. Soc. Geol. Ital. 52, 383–400.

Basili, R., Valensise, G., Vannoli, P., Burrato, P., Fracassi, U., Mariano, S., Tiberti, M.M., Boschi, E., 2008. The Database of Individual Seismogenic Sources (DISS), version 3: summarizing 20 years of research on Italy's earthquake geology. Tectonophysics 453, 20–43.

Beeler, N.M., Tullis, T.E., Blanpied, M.L., Weeks, J.D., 1996. Frictional behavior of large displacement experimental faults. J. Geophys. Res. 101, 8697–8715. http://dx.doi.org/10.1029/96JB00411.

Billi, A., Salvini, F., Storti, F., 2003. The damage zone-fault core transition in carbonate rocks: implications for fault growth, structure and permeability. J. Struct. Geol. 25, 1779–1794.

Boncio, P., Brozzetti, F., Lavecchia, G., 2000. Architecture and seismotectonics of a regional low-angle normal fault zone in central Italy. Tectonics 19, 1038–1055.

Bonson, C.G., Childs, C., Walsh, J.J., Schopfer, M.P.J., Carboni, V., 2007. Geometric and kinematic controls on the internal structure of a large normal fault in massive limestones: the Maghlaq Fault, Malta. J. Struct. Geol. 29, 336–354. http://dx.doi.org/10.1016/j.jsg.2006.06.016.

Brodsky, E.E., Jacquelyn, J., Sagy, A., Collettini, C., 2011. Faults smooth gradually as a function of slip. Earth Planet. Sci. Lett. 302, 185–193.

Bullock, R.J., De Paola, N., Holdsworth, R.E., Trabucho-Alexandre, J., 2014. Lithological controls on the deformation mechanisms operating within carbonate-hosted faults during the seismic cycle. J. Struct. Geol. 58, 22–42.

Burchfiel, B.C., Royden, L.H., van der Hilst, R.D., Heger, B.H., 2008. A geological and geophysical context for the Wenchuan earthquake of 12 May 2008, Sichuan, People's Republic of China. GSA Today 18, 4–11.

Caine, J.S., Evans, J.P., Forster, C.B., 1996. Fault zone architecture and permeability structure. Geology 24, 1025–1028.

Carpenter, B.M., Viti, C., Collettini, C., 2013. Relating Mechanical Behavior and Microstructural Observations in Calcite Fault Gouge. AGU Fall Meeting S33D-2445.

Chester, F.M., Chester, J.S., 1998. Ultracataclasite structure and friction processes of the Punchbowl fault, San Andreas system, California. Tectonophysics 295, 199–221.

Chester, F.M., Logan, J.M., 1986. Composite planar fabric of gouge from the Punchbowl fault, California. J. Struct. Geol. 9, 621–634.

Chiaraluce, L., 2012. Unravelling the complexity of Apenninic extensional fault systems: a review of the 2009 L'Aquila earthquake (Central Apennines, Italy). J. Struct. Geol. 42, 2–18. http://dx.doi.org/10.1016/j.jsg.2012.06.007.

Chiaraluce, L., Ellsworth, W.L., Chiarabba, C., Cocco, M., 2003. Imaging the complexity of an active normal fault system: the 1997 Colfiorito (Central Italy) case study. J. Geophys. Res. 108, 2294. http://dx.doi.org/10.1029/2002JB002166.

Chiaraluce, L., Barchi, M.R., Collettini, C., Mirabella, F., Pucci, S., 2005. Connecting seismically active normal faults with Quaternary geological structures: the Colfiorito 1997 case history (Northern Apennines, Italy). Tectonics 24, TC1002. http://dx.doi.org/10.1029/2004TC001627.

Ciaccio, M., Barchi, M.R., Chiarabba, C., Mirabella, F., Stucchi, E., 2005. Seismological, geological and geophysical constraints for the Gualdo Tadino fault, Umbria-Marche apennines (Central Italy). Tectonophysics 406, 233–247. http://dx.doi.org/10.1016/j.tecto.2005.05.027.

Collettini, C., Holdsworth, R.E., 2004. Fault zone weakening and character of slip along low-angle normal faults: insights from the Zuccale fault, Elba, Italy. J. Geol. Soc. 161, 1039–1051.

Collettini, C., Barchi, M.R., Chiaraluce, L., Mirabella, F., Pucci, S., 2003. The Gubbio fault: can different methods give pictures of the same object? J. Geodyn. 36, 51–66.

Collettini, C., De Paola, N., Faulkner, D.R., 2009. Insights on the geometry and mechanics of the Umbria-Marche earthquakes (Central Italy) from the integration of field and laboratory data. Tectonophysics. ISSN: 0040-1951 476, 99–109. http://dx.doi.org/10.1016/j.tecto.2008.08.013.

Collettini, C., Viti, C., Tesei, T., Mollo, S., 2013. Thermal decomposition along natural faults during earthquakes. Geology 41, 927–930. http://dx.doi.org/10.1130/G34421.1.

Cooper, M., 2007. Structural style and hydrocarbon prospectivity in fold and thrust belts: a global review. In: Ries, A.C., et al. (Eds.), Deformation of the Continental Crust: the Legacy of Mike Coward, vol. 272. Geological Society of London Special Publication, pp. 447–472.

Cowie, P.A., Roberts, G.P., 2001. Constraining slip rates and spacings of active Normal faults. J. Struct. Geol. 23, 1901–1903.

Cowie, P.A., Scholz, C.H., 1992. Growth of faults by accumulation of seismic slip. J. Geophys. Res. 97, 11085–11096.

Dawers, N.H., Anders, M.H., Scholz, C.H., 1993. Growth of normal faults: displacement-length scaling. Geology 21, 1107–1110.

De Paola, N., Collettini, C., Trippetta, F., Barchi, M.R., Minelli, G., 2007. A mechanical model for complex fault patterns induced by evaporite dehydration and cyclic changes in fluid pressure. J. Struct. Geol. 29, 1573–1584.

De Paola, N., Collettini, C., Faulkner, D.R., Trippetta, F., 2008. Fault zone architecture and deformation processes within evaporitic rocks in the upper crust. Tectonics 27. http://dx.doi.org/10.1029/2007TC002230.

De Paola, N., Hirose, T., Mitchell, T., Di Toro, G., Viti, C., Shimamoto, T., 2011. Fault lubrication and earthquake propagation in thermally unstable rocks. Geology 39, 35–38.

De Paola, N., Holdsworth, R.E., Viti, C., Collettini, C., Faoro, I., Bullock, R., 2014. Superplastic flow lubricates carbonate faults during earthquake slip. EGU Geophys. Res. Abstr. 16. EGU2014–15340.

Di Toro, G., Han, R., Hirose, T., De Paola, N., Nielsen, S., Mizoguchi, K., Ferri, F., Cocco, M., Shimamoto, T., 2011. Fault lubrication during earthquakes. Nature 471, 495–498.

D'Agostino, N., Jackson, J.A., Dramis, F., Funicello, R., 2001. Interactions between mantle upwelling, drainage evolution and active normal faulting: an example from the central Apennines (Italy). Geophys. J. Int. 147, 475–497.

Elter, P., Giglia, G., Tongiorgi, M., Trevisan, L., 1975. Tensional and contractional areas in recent Tortonian to present evolution of the Northern Apennines. Boll. Geofis. Teor. Appl. 17, 3–18.

Faulkner, D.R., Lewis, A.C., Rutter, E.H., 2003. On the internal structure and mechanics of large strike-slip faults: field observations from the Carboneras fault, south-eastern Spain. Tectonophysics 367, 235–251.

Faulkner, D.R., Jackson, C.A.L., Lunn, R.J., Schlische, R.W., Shipton, Z.K., Wibberley, C.A.J., Withjack, M.O., 2010. A review of recent developments concerning the structure, mechanics and fluid flow properties of fault zones. J. Struct. Geol. 32, 1557–1575. http://dx.doi.org/10.1016/j.jsg.2010.06.009.

Fondriest, M., Smith, S.A.F., Candela, T., Nielsen, S.B., Mair, K., Di Toro, G., 2013. Mirror like faults and power dissipation during earthquakes. Geology 41, 1175–1178.

Govoni, A., Marchetti, A., De Gori, P., Di Bona, M., Lucente, F., Improta, L., Chiarabba, C., Nardi, A., Margheriti, L., Piana Agostinetti, N., Di Giovambattista, R., Latorre, D., Anselmi, M., Ciaccio, M.G., Moretti, M., Castellano, C., Piccinini, D., 2014. The 2012 Emilia seismic sequence (Northern Italy): imaging the thrust fault system by accurate aftershock location. Tectonophysics 622, 44–55. http://dx.doi.org/10.1016/j.tecto.2014.02.013.

Gratier, J.-P., Dysthe, D., Renard, F., 2013. The role of pressure solution creep in the ductility of the Earth's upper crust. Adv. Geophys. 54, 47–179.

Han, R., Shimamoto, T., Hirose, T., Ree, J.H., Ando, J., 2007. Ultralow friction of carbonate faults caused by thermal decomposition. Science 316, 878–881.

Han, R., Hirose, T., Shimamoto, T., 2010. Strong velocity weakening and powder lubrication of simulated carbonate faults at seismic slip rates. J. Geophys. Res. 115, B03412. http://dx.doi.org/10.1029/2008JB006136.

Iacopini, D., Butler, R.W.H., 2011. Imaging deformation in submarine thrust belts using seismic attributes. Earth Planet. Sci. Lett. 302, 414–422.

Logan, J.M., Friedman, M., Higgs, N., Dengo, C., Shimamoto, T., 1979. Experimental studies of simulated fault gouge and their application to studies of natural fault zones. In: Proceedings of Conference VIII—Analysis of Actual Fault Zones in Bedrock. US Geological Survey. Open-file Report 79-1239101–120.

Long, J.J., Imber, J., 2012. Strain compatibility and fault linkage in relay zones on normal faults. J. Struct. Geol. 36, 16–26.

Maerten, L., Willemse, M.J., Pollard, D.D., Rawnsley, K., 1999. Slip distributions on intersecting normal faults. J. Struct. Geol. 21, 259–271.

Micarelli, L., Benedicto, A., Wibberley, C.A.J., 2006. Structural evolution and permeability of normal fault zones in highly porous carbonate rocks. J. Struct. Geol. 28, 1214–1227.

Miller, S.A., Collettini, C., Chiaraluce, L., Cocco, M., Barchi, M.R., Kaus, B., 2004. Aftershocks driven by a high pressure CO2 source at depth. Nature 427, 724–727.

Mirabella, F., Barchi, M., Lupattelli, A., Stucchi, E., Ciaccio, M.G., 2008. Insights on the seismogenic layer thickness from the upper crust structure of the Umbria–Marche Apennines (central Italy). Tectonics 27, 1–15. http://dx.doi.org/10.1029/2007TC002134.

Morley, C.K., Wonganan, N., 2000. Normal fault displacement characteristics, with particular reference to synthetic transfer zones, Mae Moh mine, northern Thailand. Basin Res. 12, 307–327.
Nicol, A., Walsh, J.J., Watterson, J., Bretan, P.G., 1995. Three-dimensional geometry and growth of conjugate normal faults. J. Struct. Geol. 17, 847–862.
Nicol, A., Walsh, J.J., Villamor, P., Seeback, H., Berryman, K.R., 2010. Normal fault interactions, paleoearthquakes and growth in an active rift. J. Struct. Geol. 32, 1101–1113. http://dx.doi.org/10.1016/j.jsg.2010.06.018.
Nissen, E., Jackson, J., Jahani, S., Tatar, M., 2014. Zagros "phantom earthquakes" reassessed—The inter- play of seismicity and deep salt flow in the Simply Folded Belt? J. Geophys. Res. 119 http://dx.doi.org/10.1002/2013JB010796.
Patacca, E., Scandone, P., Di Luzio, E., Cavinato, G.P., Parotto, M., 2008. Structural architecture of the central Apennines: interpretation of the CROP 11 seismic profile from the Adriatic coast to the orographic divide. Tectonics 27, 1–36. http://dx.doi.org/10.1029/2005TC001917.
Peacock, D.C.P., Sanderson, D.J., 1991. Displacements, segment linkage and relay ramps in normal fault zones. J. Struct. Geol. 13, 721–733.
Ramsay, J.G., 1967. Folding and Fracturing of Rocks. McGraw-Hill, New York, p. 568.
Rowe, C.D., Fagereng, A., Miller, J.A., Mapani, B., 2012. Signature of coseismic decarbonation in dolomitic fault rocks of the Naukluft Thrust, Namibia. Earth Planet. Sci. Lett. 333, 200–210.
Sagy, A., Brodsky, E.E., Axen, G.J., 2007. Evolution of fault-surface roughness with slip. Geology 35, 283–286.
Santantonio, M., 1994. Pelagic Carbonate Platforms in the geologic record: their Classification and Sedimentary and Paleotectonic evolution. Am. Assoc. Pet. Geol. Bull. 78, 122–141.
Santantonio, M., 2006. Facies associations and evolution of pelagic carbonate platform/basin systems: examples from the Italian Jurassic. Sedimentology 6, 1039–1067.
Scarsella, F., 1950. Sui rapporti stratigrafici del "Calcare massiccio" (Calcare di scogliera Hettangiano) con i sovrastanti piani stratigrafici della serie Giura-Liassica nell'Appennino Umbro-Marchigiano. B. Soc. Geol. Ital. 69, 96–98.
Schlische, R.W., Young, S.S., Ackermann, R.V., Gupta, A., 1996. Geometry and scaling relations of a population of very small rift-related faults. Geology 24, 683–686.
Scholz, C.H., 2002. The Mechanics of Earthquakes and Faulting, second ed. Cambridge University Press, pp. 1–508.
Scholz, C.H., Gupta, A., 2000. Fault interactions and seismic hazard. J. Geodyn. 29, 459–467.
Scuderi, M.M., Niemeijer, A., Collettini, C., Marone, C., 2013. Frictional properties and slip stability of active faults within carbonate-evaporite sequences: the role of dolomite and anhydrite. Earth Planet. Sci. Lett. 369, 220–232.
Serpelloni, E., Faccenna, C., Spada, G., Dong, D., Williams, S.D.P., 2013. Vertical GPS ground motion rates in the Euro-Mediterranean region: new evidence of velocity gradients at different spatial scales along the Nubia-Eurasia plate boundary. J. Geophys. Res. 118, 6003–6024. http://dx.doi.org/10.1002/2013JB010102.
Sibson, R.H., 1977. Fault rocks and fault mechanisms. J. Geol. Soc. Lond. 133, 191–213.
Sibson, R.H., 1992. Implications of fault-valve behaviour for rupture nucleation and recurrence. Tectonophysics 211, 283–293.
Siman-Tov, S., Aharonov, E., Sagy, A., Emmanuel, S., 2013. Nanograins form carbonate fault mirrors. Geology 41, 703–706. http://dx.doi.org/10.1130/G34087.1.
Smith, S.A.F., Billi, A., Di Toro, G., Spiess, R., 2011. Principal slip zones in limestone: microstructural characterization and implications for the seismic cycle (Tre Monti Fault, Central Apennines, Italy). Pure Appl. Geophys. 168, 2365–2393. http://dx.doi.org/10.1007/s00024-011-0267-5.
Smith, S.A.F., Di Toro, G., Kim, S., Ree, J.H., Nielsen, S., Billi, A., Spiess, R., 2013. Coseismic recrystallization during shallow earthquake slip. Geology 41, 63–66.
Stewart, I.S., Hancock, P.L., 1991. Scales of structural heterogeneity within neotectonic normal fault zones in the Aegean region. J. Struct. Geol. 13, 191–204.
Tchalenko, J.S., 1970. Similarities between shear zones of different magnitudes. Bull. Geol. Soc. Am. 81, 1625–1640.
Tesei, T., Collettini, C., Viti, C., Barchi, M.R., 2013. Fault architecture and deformation mechanisms in exhumed analogues of seismogenic carbonate-bearing thrusts. J. Structutal Geology 55, 167–181.
USGS, 2000. US Geological Survey World Petroleum Assessment 2000—Description and Results [CD- ROMs]. USGS Digital data series DDS-60.
Valoroso, L., Chiaraluce, L., Collettini, C., 2014. Earthquakes and fault zone structure. Geology 42, 343–346.
Verberne, B.A., de Bresser, J.H.P., Niemeijer, A.R., Spiers, C.J., Winter, D.A.M., Plümper, O., 2013. Nanocrystalline slip zones in calcite fault gouge show intense crystallographic preferred orientation: crystal plasticity at sub-seismic slip rates at 18–150 °C. Geology 41, 863–866.
Violay, M., Nielsen, S., Gibert, B., Spagnulo, E., Cavallo, A., Azais, P., Vinciguerra, S., Di Toro, G., 2013. Pore fluid in experimental calcite-bearing faults: abrupt weakening and geochemical signature of co-seismic processes. Earth Planet. Sci. Lett. 361, 74–84. http://dx.doi.org/10.1016/J.Epsl.2012.11.021.
Viti, C., Collettini, C., Tesei, T., 2014. Pressure solution seams in carbonatic fault rocks: mineralogy, micro/nanostructures and role in deformation mechanism. Contrib. Mineral. Petr. 167, 1–15. http://dx.doi.org/10.1007/s00410-014-0970-1.
Walsh, J.J., Nicol, A., Childs, C., 2002. An alternative model for the growth of faults. J. Struct. Geol. 24, 1669–1675.
Wibberley, C.A.J., Yielding, G., Di Toro, G., 2008. Recent advances in the understanding of fault zone internal structure; a review. In: Wibberley, C.A.J., Kurz, W., Imber, J., Holdsworth, R.E., Collettini, C. (Eds.), Structure of Fault Zones: Implications for Mechanical and Fluid-flow Properties, 299. Geological Society of London Special Publication, pp. 5–33.
Wintsch, R.P., Christoffersen, R., Kronenberg, A.K., 1995. Fluid-rock reaction weakening of fault zones. J. Geophys. Res. 100, 13021–13032.